JACS
JOURNAL OF THE AMERICAN CHEMICAL SOCIETY
pubs.acs.org/JACS

Article

Enantiomerically Pure Helical Bilayer Nanographenes: A Straightforward Chemical Approach

Patricia Izquierdo-García, Jesús M. Fernández-García, Josefina Perles, and Nazario Martín*

Cite This: J. Am. Chem. Soc. 2024, 146, 34943−34949

Read Online

ACCESS | Metrics & More | Article Recommendations | Supporting Information

ABSTRACT: The semiconductor properties of nanosized graphene fragments, known as molecular nanographenes, position them as exceptional candidates for next-generation optoelectronics. In addition to their remarkable optical and electronic features, chiral nanographenes exhibit high dissymmetry factors in circular dichroism and circularly polarized luminescence measurements. However, the synthesis of enantiomerically pure nanographenes remains a significant challenge. Typically, these materials are synthesized in their racemic form, followed by separation of the enantiomers using high-performance liquid chromatography (HPLC). While effective, this method often requires expensive instrumentation, extensive optimization of separation conditions, and typically yields analytical quantities of the desired samples. An alternative approach is the enantioselective synthesis of chiral molecular nanographenes; however, to date, only two examples have been documented in the literature. In this work, we present a straightforward chemical method for the chiral resolution of helical bilayer nanographenes. This approach enables the effective and scalable preparation of enantiomerically pure nanographenes while avoiding the need for HPLC. The incorporation of a BINOL core into the polyarene precursor facilitates the separation of diastereomers through esterification with enantiomerically pure camphorsulfonyl chloride. Following the separation of the diastereomers by standard chromatographic column, the hydrolysis of the camphorsulfonyl group yields enantiomerically pure nanographene precursors. The subsequent graphitization, achieved through the Scholl reaction, occurs in an enantiospecific manner and with the concomitant formation of a furan ring and a heterohelicene moiety. The absolute configurations of the final enantiomers, *P*-**oxa**[**9**]**HBNG** and *M*-**oxa**[**9**]**HBNG**, have been determined using X-ray diffraction. Additionally, electrochemical, photophysical, and chiroptical properties have been thoroughly evaluated.

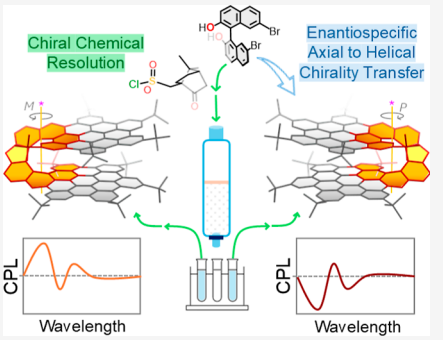

INTRODUCTION

Molecular nanographenes (NGs) have emerged as promising candidates for the advancement of innovative optoelectronic devices,[1] primarily attributable to their semiconductor features stemming from the quantum confinement of electrons at the nanoscale.[2] By using the arsenal of modern organic reactions, the bottom-up synthesis[3] of these carbon-based materials enables the tailored production of molecular structures in customizable sizes,[4] shapes,[5] and consequently, properties at will.

Chiral NGs have recently attracted significant attention due to the interplay between their inherent chirality and the optical and electronic properties they exhibit.[6] In this regard, the π-extension of these molecules not only enhances their properties as excellent fluorophores but also improves the dissymmetry factors controlling the chiroptical properties, namely circular dichroism (CD) and circularly polarized luminescence (CPL).[7] In recent years, numerous research groups have synthesized a variety of NGs that incorporate helical motifs, such as helicenes,[8] resulting in molecules with propeller-like shapes[9] or forming helical bilayers.[10]

Similar to the observation that graphene bilayers modify their electronic structure,[11] exhibiting superconductivity by twisting a specific "magic angle",[12] helical bilayer NGs (HBNGs) have shown to alter their electronic properties depending on the overlapping degree of both layers.[13]

This intriguing behavior highlights the potential of helical bilayer NGs (HBNGs) for innovative applications in electronics and photonics, exploiting also their chirality,[14] thus paving the way to a new and less-explored scenario. However, the main limitation to address this challenge stems from the difficulty in obtaining enantiomerically pure NGs. Typically, this has mostly been accomplished through high-performance liquid chromatography (HPLC) separation of racemates, a process that is both costly and time-consuming, often yielding only analytical quantities of the desired enantiomerically pure samples, thus preventing their use for practical purposes.

Received: October 16, 2024
Revised: November 25, 2024
Accepted: November 27, 2024
Published: December 6, 2024

https://doi.org/10.1021/jacs.4c14544
J. Am. Chem. Soc. 2024, 146, 34943−34949

Chart 1. Approaches to Enantiomerically Pure Chiral Bilayer NGs

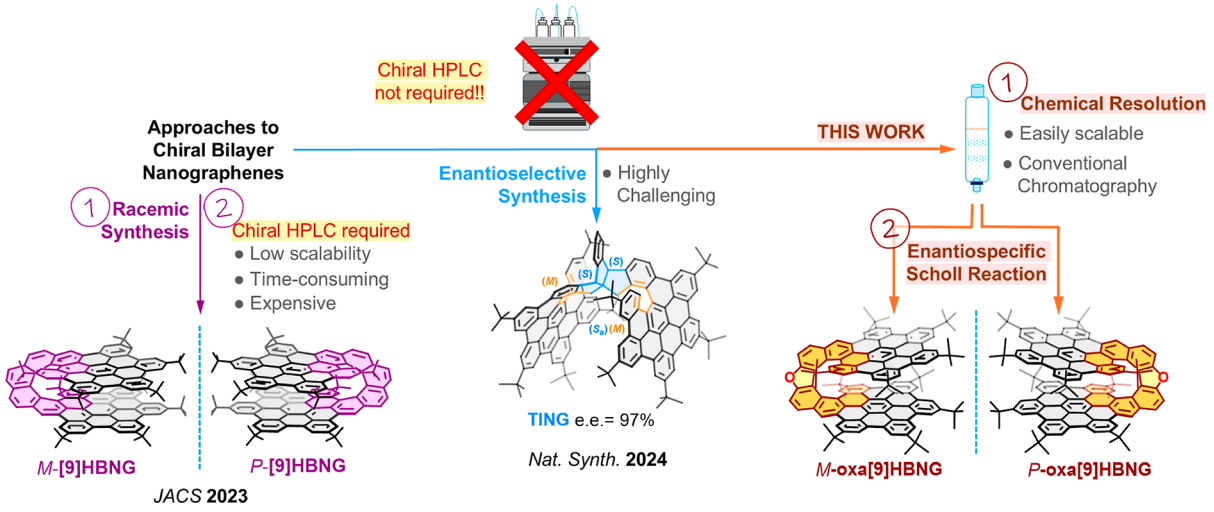

One approach to address this issue is to carry out an enantioselective synthesis of chiral NGs. To the best of our knowledge, only two examples have very recently been described in the literature thus far. Last year, our research group made significant advances by pioneering the enantioselective synthesis of triindane-based molecular NGs (TING, Chart 1).[15] A few months later, Tanaka et al. published a second example detailing the enantiomeric synthesis of π-extended carbohelicenes.[16] These methodologies present the opportunity to produce substantial quantities of enantiomerically pure NGs, which are essential for their further application in devices.

In this work, we introduce an alternative and straightforward approach that employs a chemical resolution to synthesize enantiomerically pure helical bilayer NGs through a methodology characterized by its scalability and efficiency, avoiding the use of the HPLC technique. Thus, starting from a commercially available naphthol halide to synthesize a π-extended BINOL, and taking advantage of the high stability of this derivative against racemization,[17] we employ an esterification reaction with an enantiomerically pure camphorsulfonyl chloride. This approach enables the chemical resolution of the resulting diastereomers through straightforward standard chromatographic column techniques. Subsequent hydrolysis and graphitization steps yield two enantiomerically pure helical bilayer NGs *M*-**oxa[9]HBNG** and *P*-**oxa[9]HBNG**. Single crystal X-ray diffraction determines the absolute configuration of the final products and the enantiospecificity of the final graphitization step. Furthermore, cyclic voltammetry experiments confirm the mixed valence effect of these novel bilayers. Additionally, the study of photophysical and chiroptical properties reveal significant dissymmetry factors, highlighting the singular features of these materials.

RESULTS AND DISCUSSION

Racemic Synthetic Procedure. The synthetic methodology starts from commercially available 7-bromo-2-naphthol (**1**). Thus, as detailed in Scheme 1, the first step is an oxidative homocoupling of **1**, mediated by a Cu-TMDA catalyst, affording 7,7′-dibromo-1,1′-binaphthyl-2,2′-diol (**2**, 83%). Then, a 2-fold Sonogashira coupling between **2** and two equivalents of 4-(*tert*-butyl)phenylacetylene (**3**) is performed, providing 7,7′-bis[(4-(*tert*-butyl)phenyl)ethynyl]-1,1′-binaphthalyl-2,2′-diol (**4**, 96%). The resulting alkynyl containing BINOL **4** was reacted with cyclopentadienone **5** to perform a double Diels−Alder cycloaddition, after in situ carbon monoxide extrusion, the BINOL-based polyarene endowed with two penta(4-*tert*-butylphenyl)phenyl groups **6** is obtained with a remarkably good yield of 93%. The incorporation of a BINOL core into the structure, provides great versatility considering the configurational stability of the isomers (racemization barrier 38 kcal·mol^{-1}).[17a] Finally, a Scholl cyclodehydrogenation using DDQ as oxidant and triflic acid as Brønsted acid is performed, affording a furan-embedded helicene backbone, and thus, the helical bilayer NG **oxa[9]-HBNG** in 61% yield. During the last step, 12 carbon−carbon bonds are formed providing the graphitization of **6**. In addition, the cyclodehydration of the phenol groups results in the formation of a carbon−oxygen bond leading to the closure of the furan ring.[18] This reactivity to form furan embedded oxa-helicenes[19] provides the possibility of modulating, and improving the optoelectronic and chiroptical properties, as demonstrated by different studies of heterohelicenes.[20]

Scheme 1. Synthesis of Racemic Oxa[9]HBNG from 7-Bromo-2-naphthol

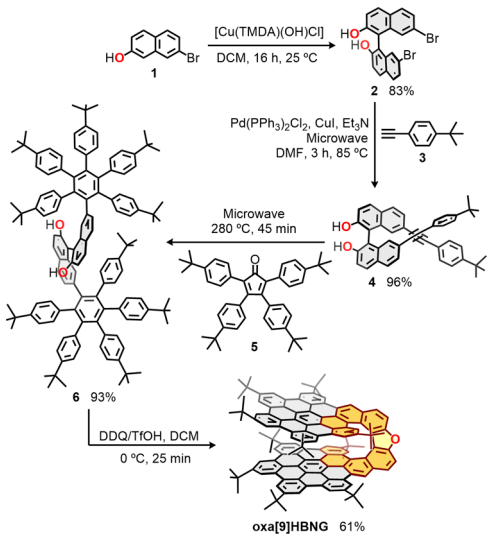

https://doi.org/10.1021/jacs.4c14544
J. Am. Chem. Soc. 2024, 146, 34943−34949

The final product and all nondescribed intermediates, were completely characterized by NMR, HRMS and FT-IR. The ^{1}H NMR of **oxa[9]HBNG** exhibits 11 singlets and two doublets at low field corresponding to the aromatic protons, and five singlets at high field corresponding to the *tert*-butyl groups (Figure S7, see Supporting Information). The number of signals reveals the symmetry of the structure due to a C_2 axis. As can be seen, the expected phenol signal between 3.50 and 4.00 ppm does not appear in the spectrum, which is evidence of closure to form the furan cycle. In addition, mass spectrometry experiments show the loss of 42 units from **6** (exact mass, 1759.1040) to **oxa[9]HBNG** (exact mass, 1716.8948), which agrees to the formation of 12 C−C bonds (24 units), and the loss of 18 units due to cyclodehydration to form a new C−O bond.

Chemical Resolution and Enantiospecific Scholl Reaction. The enantiomerically pure preparation of **oxa[9]-HBNGs** starts with the monoesterification of the polyarene **6** with 1*R*-10-camphorsulfonyl chloride (Scheme 2), affording

Scheme 2. Chemical Resolution of Racemate 6 and Enantiospecific Synthesis of *M*-oxa[9]HBNG and *P*-oxa[9]HBNG

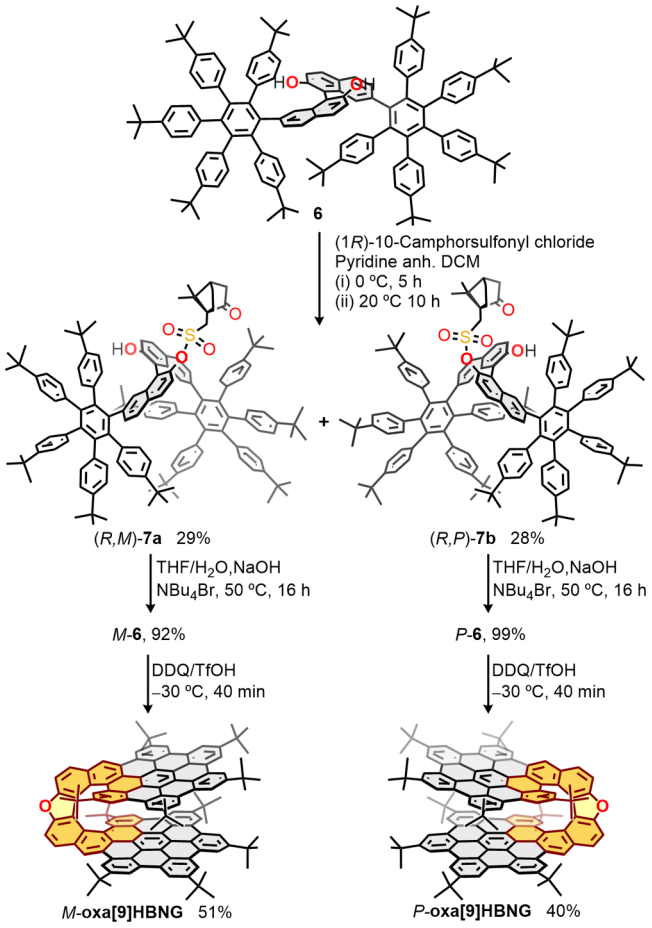

two diastereomers, *R,M*-**7a** (29%) and *R,P*-**7b** (28%) easily isolable by silica gel column chromatography. The purity of the diastereomers was determined by 500 MHz ^{1}H NMR, revealing an excellent isolation (purity >95% for both diastereomers, Figures S4 and S5, see Supporting Information). Polyarene diastereomeric derivatives *R,M*-**7a** and *R,P*-**7b** show clear differences by NMR, as expected from diastereomers (Figure S6, see Supporting Information). The substitution with only one camphorsulfonyl group entails a great asymmetry in the spectra, each diastereomer presents ten singlets, between 1.11 and 1.00 ppm, corresponding to the *tert*-butyl groups, whereas the starting polyarene **6** exhibits only five singlets (Figure S3, see Supporting Information), revealing the symmetry loss after the functionalization.

Enantiopure crystals of *R,P*-**7b**, were obtained from a chloroform solution, allowing its structure to be solved by single crystal X-ray diffraction (Figure 1 and Table S1, see

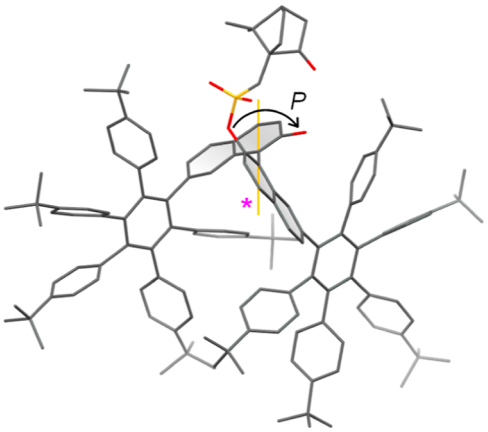

Figure 1. X-ray structure of *R,P*-**7b** showing the chiral auxiliar, 1*R*-10-camphorsulphonil, and the *P* configuration of the binaphthol core.

Supporting Information). The molecules crystallize in the $P2_12_12_1$ space group, and its absolute configuration was unequivocally assigned based on the value of Flack and Hooft parameters. The absence of relevant $\pi-\pi$ or C−H$\cdots\pi$ intramolecular interactions entails a high degree of disorder in several fragments of the molecule, especially relevant for some of the peripheral *tert*-butyl groups. The packing in the crystal is achieved by weak van der Waals forces, leaving large interstitial spaces that contain disordered solvent molecules.

Once separated, the camphorsulfonyl group of each diasteromer is removed by basic hydrolysis reactions, affording enantiomerically pure BINOL-based polyarenes *M*-**6** (92%)and *P*-**6** (99%). The hydrolysis conditions to afford *M*-**6** and *P*-**6** are mild enough to prevent racemization. Finally, the Scholl reaction providing the helical bilayer NG **oxa[9]-HBNG** occurs enantiospecifically. The configurationally stable atropisomers *M*-**6** and *P*-**6** are transformed into helically full-conjugated NGs with axial-to-helical chirality transfer, leading to enantiomerically pure *M*-**oxa[9]HBNG** (51%) and *P*-**oxa[9]HBNG** (40%), respectively.

The enantiomeric excess of the *M*- and *P*-**oxa[9]HBNG** were evaluated by chiral HPLC (*R,R*-Whelk O2 5 μm column, 70% hexane 30% chloroform, recording the absorption by UV−vis and CD at 375 nm, Section 6, see Supporting Information), showing an e.e. >99% for *M*-**oxa[9]HBNG** and e.e. >99% for *P*-**oxa[9]HBNG**. Considering the total enantiospecificity of the Scholl reaction, the enantiomeric excesses depend only on the enantiopurity of the starting materials *M*-**6** and *P*-**6**, determined by the proper separation of the diastereomers by silica gel chromatographic column.

The structures of *P*-**oxa[9]HBNG** and *M*-**oxa[9]HBNG** were solved by single crystal X-ray diffraction (Figure 2 and Table S2, see Supporting Information) from enantiopure crystals. Each of the compounds crystallize in the $C222_1$

https://doi.org/10.1021/jacs.4c14544
J. Am. Chem. Soc. 2024, 146, 34943−34949

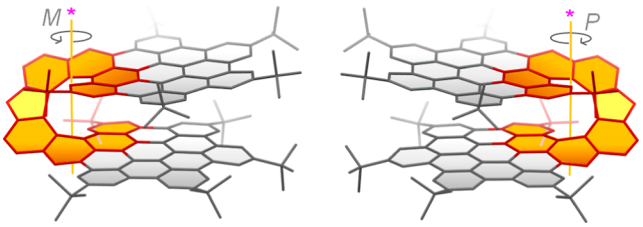

Figure 2. X-ray crystal structures of *M*-**oxa**[**9**]**HBNG** and *P*-**oxa**[**9**]**HBNG** showing the inherent configuration of the helicene moieties.

Sohncke space group, with one-half of the molecule in the asymmetric unit. Their absolute configuration was unambiguously assigned by the Bayesian statistical analysis on Bijvoet pairs differences.

Both molecules of **oxa**[**9**]**HBNGs** display a bent U-shape where the two layers are placed almost parallel to each other (4.34° angle for *P*-**oxa**[**9**]**HBNG** and 4.95° for *M*-**oxa**[**9**]-**HBNG**) maximizing the overlap of the two NG fragments (Figure S12, see Supporting Information). As many as 12 rings in each layer retain an overall flat disposition (Table S3, see Supporting Information), and 10 of them are involved in strong $\pi-\pi$ interactions, with an average distance of 3.61 Å (*P*-**oxa**[**9**]**HBNG**) and 3.63 Å (*M*-**oxa**[**9**]**HBNG**) between the centroids of a layer and the plane defined by the ones in the opposite layer (Table S4, see Supporting Information). Regarding the supramolecular arrangement, the molecules are located in sheets parallel to the (110) plane and separated by a distance of $c/2$, with the **oxa**[**9**]**HBNG** molecules facing alternatingly the [010] and [0−10] directions (see Figure S11, see Supporting Information). The huge spaces left between the layers contain highly disordered solvent molecules.

Electrochemical Properties. The electrochemical properties of **oxa**[**9**]**HBNG** were evaluated by cyclic voltammetry in a 0.1 M solution of tetrabutylammonium hexafluorophosphate in toluene/acetonitrile 4:1 using glassy carbon as working electrode, a reference electrode of $Ag/AgNO_3$, and a platinum wire as counter electrode. The oxidation and reduction potentials vs Fc/Fc^+ are shown in Figure 3, **oxa**[**9**]**HBNG** presents two quasi-reversible oxidation waves at $E_{1/2ox}{}^1 = 0.37$ V and $E_{1/2ox}{}^2 = 0.66$ V, and two quasi-reversible reduction

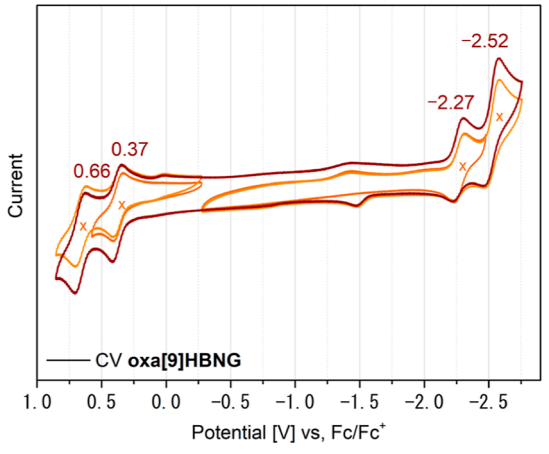

Figure 3. Cyclic voltammogram of **oxa**[**9**]**HBNG** showing its half-wave redox potentials vs Fc/Fc^+ in a 1 M solution of tetrabutylammonium hexafluorophosphate in toluene/acetonitrile 4:1.

waves $E_{1/2red}{}^1 = -2.27$ V and $E_{1/2red}{}^2 = -2.52$ V. As commented in the introduction, graphene-like bilayers show exotic electronic properties depending on the relative disposition between the graphitized layers. In this way, HBNGs show mixed valence effects strongly related to the overlapping degree between the layers.[13] In the case of **oxa**[**9**]**HBNG**, the mixed valence band effect stabilizes the radical cation formed in the first oxidation between the layers, eventually decreasing the oxidation potential to 0.37 V. This value is comparable with the first oxidation potential of [**9**]**HBNG** $E_{1/2ox}{}^1 = 0.35$ V (Chart 1),[13] a highly overlapped helical bilayer NG with high contribution of mixed valence effects. Furthermore, comparing the first oxidation wave with that of an oxa[7]helical NG reported by Jux et al., in which the HBC layers do not show intramolecular $\pi-\pi$ interactions ($E_{1/2ox}{}^1 = 0.9$ V),[21] **oxa**[**9**]**HBNG** shows a significantly stronger donor character. Therefore, it can be concluded that the contribution of heteroatom in the helicene has a low impact over the oxidation potential, being the strong donor character of **oxa**[**9**]**HBNG** attributed to the mixed valence effect derived from the overlapping between the layers (20 rings involved in the $\pi-\pi$ interactions, Table S4, see Supporting Information). DFT calculations indicate that the HOMO orbital is primarily localized on the helicene moiety as expected, due to the electron-donating character of the furan ring. However, the HOMO−1 orbital, which is close in energy, is localized on the HBC layers, thus contributing to the observed mixed-valence effects (see Figure S17).[13]

However, the oxygen embedded in the helicene seems to be more important regarding the electron acceptor character of **oxa**[**9**]**HBNG**. The LUMO orbital of the carbon-based NG, [**9**]**HBNG**, is mainly located in the helicene backbones.[22] In the case of **oxa**[**9**]**HBNG**, the electron-donor character of both the helicene (due to the electron-donor character of the furan ring), and the hexa-*peri*-hexabenzocoronene (HBC) layers, entails the destabilization of the LUMO orbital (see Figure S17). Thus, the potential of the first reduction wave increases (in absolute value) to $E_{1/2red}{}^1 = -2.27$ V, revealing a weaker electron acceptor character vs [**9**]HBNG ($E_{1/2red}{}^1 = -2.18$ V).

Photophysical Properties of the Racemic Mixture. The photophysical properties of **oxa**[**9**]**HBNG** were evaluated by UV−vis absorption and emission measurements in chloroform (Figure 4). The absorption spectrum of **oxa**[**9**]-**HBNG** displays nonstructured broad bands in the ultraviolet region of the absorption spectrum (344, 371, 398 nm) very similar to those of the previously described [**9**]**HBNG**,[13] and more structured weak bands in the visible region (450, 476, 498 nm).

The emission spectrum of **oxa**[**9**]**HBNG** shows well-structured bands with maxima at 500, 537, and 580 nm, which contrasts with the excimer-like broad bands displayed by [**9**]**HBNG**.[13] As illustrated in Figure 4, the emission bands of **oxa**[**9**]**HBNG** (orange shaded curve) are blue-shifted with respect to the previously described carbon-based [**9**]**HBNG** (purple shaded curve), and are more comparable to those of the hexa-*tert*-butyl-substituted HBC (^{t}Bu-HBC, blue shaded curve). These observations agree with the cyclic voltammetry data previously described. The incorporation of the oxygen atom in the helicene modifies the structure and entails the modification of the LUMO orbital, which is not farther localized in the helicene moiety, as for carbon-based [**9**]**HBNG**. This modification involves the variation of the the photophysical properties, and the emission bands are no longer

https://doi.org/10.1021/jacs.4c14544
J. Am. Chem. Soc. 2024, 146, 34943−34949

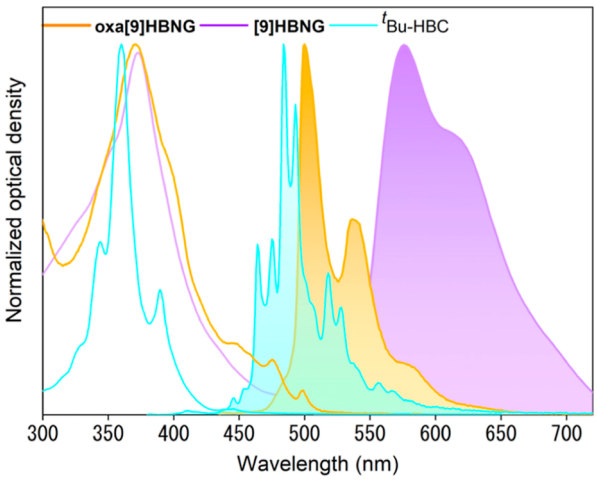

Figure 4. Absorption (solid lines) and emission (shaded curves) spectra of **oxa**[9]**HBNG** and [9]**HBNG** in chloroform.

excimer-like. The fluorescence quantum yield of **oxa**[9]**HBNG** resulted of Φ_{em} = 0.30, determined by comparison with the emission spectra of fluoresceine in ethanol (Φ_{em} = 0.97) at 432 nm. The optical band gap calculated in the intersection of the absorption and emission spectra E_{0-0} = 2.55 eV, clearly fits with the electrochemical band gap E = 2.51 eV, resulting from the difference between the electron affinity and the ionization potential (Figure S14, see Supporting Information). This value is also comparable to the HOMO−LUMO gap obtained from DFT calculations, which is 2.93 eV (Figure S17).

Chiroptical Properties of Enantiomerically Pure HBNGs. The electronic circular dichroism (CD) has been recorded in chloroform for both enantiomerically pure NGs *M*-**oxa**[9]**HBNG** and *P*-**oxa**[9]**HBNG**. As illustrated in Figure 5,

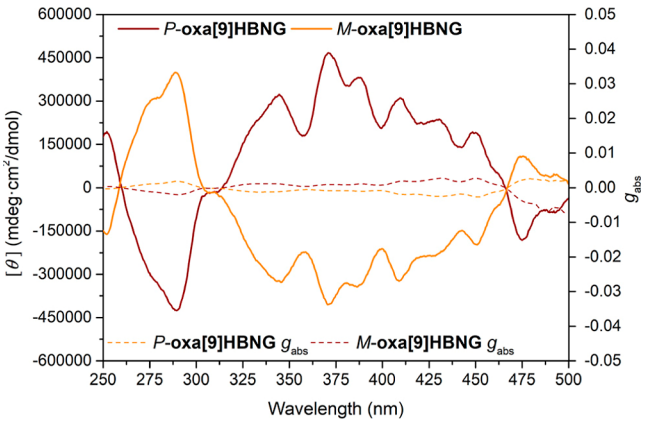

Figure 5. CD spectra and g_{abs} values of *M*-**oxa**[9]**HBNG** and *P*-**oxa**[9]**HBNG**.

the spectra of the enantiomers (*P*-**oxa**[9]**HBNG**, brown solid line, and *M*-**oxa**[9]**HBNG**, orange solid line) show specular image signals and two main regions with prominent Cotton effects. One intense broad band from the ultraviolet region to the visible region (300 to 470 nm), and one of lower intensity at lower energy in the visible region (480 nm). The absorption dissymmetry factors represented with dashed lines in Figure 5, are $g_{abs} = -2.7 \times 10^{-3}$ at 452 nm for *M*-**oxa**[9]**HBNG**, and $g_{abs} = +2.6 \times 10^{-3}$ at 452 nm for *P*-**oxa**[9]**HBNG**.

The CPL has also been recorded in chloroform for both enantiomerically pure NGs *M*-**oxa**[9]**HBNG** and *P*-**oxa**[9]-**HBNG** (Figure 6). Both spectra are symmetrical and show

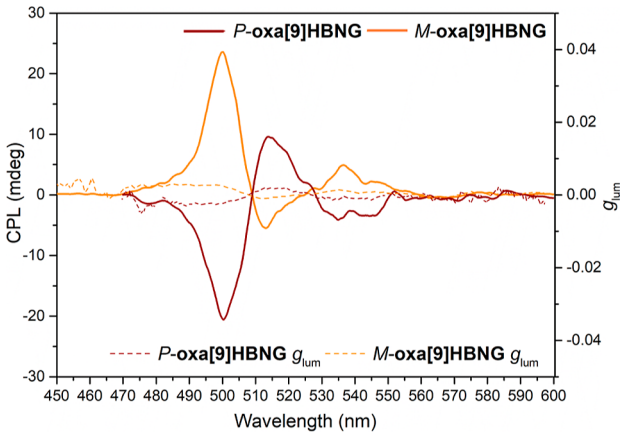

Figure 6. CPL spectra and g_{lum} values of *M*-**oxa**[9]**HBNG** and *P*-**oxa**[9]**HBNG**.

three main regions with different Cotton effects. The emission dissymmetry factors (dashed lines, Figure 6) are, $g_{lum} = +2.6 \times 10^{-3}$ at 500 nm for *M*-**oxa**[9]**HBNG**, and $g_{lum} = -2.4 \times 10^{-3}$ at 500 nm for *P*-**oxa**[9]**HBNG**. The low variation between the g_{asb} and the g_{lum} values indicates that the structures present similar geometries in the fundamental and the first excited state. Furthermore, these dissymmetry factors are in the typical range of values presented by helical NGs.

CONCLUSIONS

The synthesis of enantiomerically pure helical bilayer NGs *M*-**oxa**[9]**HBNG** and *P*-**oxa**[9]**HBNG** by an easily scalable methodology, is described. The synthesis starts from commercially available 7-bromo-2-naphthol that, in the presence of copper(II), yields axially chiral racemic dibromo-BINOL **2** which has been π-extended to the BINOL-based polyarene **6**. Taking advantage of the stable axial chirality and reactivity of the obtained BINOL-based structures, a chiral resolution was carried out by functionalizing **6** with enantiomerically pure camphorsulfonyl chloride. The separation of the obtained diastereomers *R,M*-**7a** and *R,P*-**7b** by conventional silica gel chromatographic column afforded an isomeric excess >95% (by NMR). After a hydrolysis step under mild conditions, enantiomerically pure BINOL-based polyarenes *P*- and *M*-**6** were obtained which, under Scholl reaction conditions, lead to the corresponding enantiomerically pure *P*- and *M*-**oxa**[9]**HBNG**. During the Scholl oxidation two different types of reactions take place, the expected cyclodehydrogenation (providing the graphene-like structure), and the enantiospecific cyclodehydration of the phenol groups yielding the furan embedded helicene (axial-to-helical chirality transfer). The performance of the silica column separation determines the enantiomeric excess of the final NGs (e.e. >99% by chiral HPLC for each enantiomer). All structures were characterized by spectroscopic techniques (NMR, FT-IR, HRMS) and single-crystal X-ray diffraction confirmed the configuration of the BINOL core in diastereomeric polyarene *R,P*-**7b** and the corresponding enantiomer obtained after hydrolysis and Scholl reaction, *P*-**oxa**[9]**HBNG**. Furthermore, the crystal structure of the other enantiomeric NG *M*-

https://doi.org/10.1021/jacs.4c14544
J. Am. Chem. Soc. 2024, 146, 34943−34949

oxa[9]HBNG has also been obtained. These studies showed the great overlapping between the layers, being 20 rings involved in the intramolecular $\pi-\pi$ interactions.

The large overlap of the structure explains the variation of the donor character. The influence of the electron-donor character of oxygen in the helicene backbone has a lower impact on the oxidation potentials ($E_{1/2ox}^{1}$ = 0.35 V and $E_{1/2ox}^{1}$ = 0.66 V) than the influence of the overlapping degree between the layers leading to a mixed valence band effect. The influence of the electron-donor character of the oxygen-containing helicene is more reflected in the acceptor character. Thus, the first reduction potential for **oxa[9]HBNG** ($E_{1/2red}^{1}$ = −2.27 V) is closer to that of ^{t}Bu-HBC ($E_{1/2red}^{1}$ = −2.24 V). In addition, the emission spectra show structured bands suggesting the lower excimer-like contribution. Finally, the chiroptical properties of *M*- and *P*-**oxa[9]HBNG** have been studied by means of electronic circular dichroism and circularly polarized luminescence, from which absorption and emission dissymmetry factors in the typical range of helical NGs, with g_{abs} values of -2.7×10^{-3} at 452 nm for *M*-**oxa[9]HBNG** and $+2.6 \times 10^{-3}$ at 452 nm for *P*-**oxa[9]HBNG**, and g_{lum} values of $+2.6 \times 10^{-3}$ for *M*-**oxa[9]HBNG** and -2.4×10^{-3} for *P*-**oxa[9]HBNG**.

■ ASSOCIATED CONTENT

Supporting Information

The Supporting Information is available free of charge at https://pubs.acs.org/doi/10.1021/jacs.4c14544.

Synthetic procedures, additional figures/schemes of physical properties and characterization data. Data for *R,P*-**7b** (CCDC: 2388461), *M*-**oxa[9]HBNG** (CCDC: 2388463) and *P*-**oxa[9]HBNG** (CCDC: 2388462) (PDF)

Accession Codes

Deposition numbers 2388461−2388463 contain the supplementary crystallographic data for this paper. These data can be obtained free of charge via the joint Cambridge Crystallographic Data Centre (CCDC) and Fachinformationszentrum Karlsruhe Access Structures service.

■ AUTHOR INFORMATION

Corresponding Author

Nazario Martín − *Departamento de Química Orgánica I, Facultad de Ciencias Químicas, Universidad Complutense de Madrid, 28040 Madrid, Spain; IMDEA-Nanociencia, 28049 Madrid, Spain;* orcid.org/0000-0002-5355-1477; Email: nazmar@ucm.es

Authors

Patricia Izquierdo-García − *Departamento de Química Orgánica I, Facultad de Ciencias Químicas, Universidad Complutense de Madrid, 28040 Madrid, Spain;* orcid.org/0000-0002-5004-1375

Jesús M. Fernández-García − *Departamento de Química Orgánica I, Facultad de Ciencias Químicas, Universidad Complutense de Madrid, 28040 Madrid, Spain;* orcid.org/0000-0002-7366-6845

Josefina Perles − *Laboratorio DRX Monocristal, SIdI, Universidad Autónoma de Madrid, 28049 Madrid, Spain;* orcid.org/0000-0003-0256-0186

Complete contact information is available at: https://pubs.acs.org/10.1021/jacs.4c14544

Notes

The authors declare no competing financial interest.

■ ACKNOWLEDGMENTS

P.I.-G., J.M.F.-G. and N.M. acknowledge financial support from the Spanish MICIN (project PID2020-114653RB I00), they also acknowledge financial support from the ERC (SyG TOMATTO ERC-2020-951224) and from the "(MAD2D-CM)-UCM" project funded by Comunidad de Madrid, by the Recovery, Transformation and Resilience Plan, and by NextGenerationEU from the European Union.

■ REFERENCES

(1) (a) Wang, G.; Yu, M.; Feng, X. Carbon Materials for Ion-intercalation Involved Rechargeable Battery Technologies. *Chem. Soc. Rev.* **2021**, *50*, 2388. (b) Tucek, J.; Blonski, P.; Ugolotti, J.; Swain, A. K.; Enoki, T.; Zboril, R. Emerging Chemical Strategies for Imprinting Magnetism in Graphene and Related 2D Materials for Spintronic and Biomedical Applications. *Chem. Soc. Rev.* **2018**, *47*, 3899. (c) Fresta, E.; Dosso, J.; Cabanillas-González, J.; Bonifazi, D.; Costa, R. D. Revealing the Impact of Heat Generation Using Nanographene-Based Light-Emitting Electrochemical Cells. *ACS Appl. Mater. Interfaces* **2020**, *12*, 28426. (d) Das, S.; Pandey, D.; Thomas, J.; Roy, T. The Role of Graphene and Other 2D Materials in Solar Photovoltaics. *Adv. Mater.* **2019**, *31*, No. e1802722.

(2) (a) Ritter, K. A.; Lyding, J. W. The Influence of Edge Structure on the Electronic Properties of Graphene Quantum Dots and Nanoribbons. *Nat. Mater.* **2009**, *8* (3), 235. (b) Sun, Z.; Ye, Q.; Chi, C.; Wu, J. Low Band Gap Polycyclic Hydrocarbons: from Closed-shell Near Infrared Dyes and Semiconductors to Open-Shell Radicals. *Chem. Soc. Rev.* **2012**, *41*, 7857. (c) Li, S.-Y.; He, L. Recent Progresses of Quantum Confinement in Graphene Quantum Dots. *Front. Phys.* **2021**, *17*, 33201. (d) Arimura, S.; Matsumoto, I.; Sekiya, R.; Haino, T. Intermediate Color Emission via Nanographenes with Organic Fluorophores. *Angew. Chem., Int. Ed.* **2024**, *63*, No. e202315508. (e) Sekiya, R.; Haino, T. Edge-Functionalized Nanographenes. *Chem.—Eur. J.* **2021**, *27*, 187−199.

(3) (a) Grzybowski, M.; Sadowski, B.; Butenschon, H.; Gryko, D. T. Synthetic Applications of Oxidative Aromatic Coupling-From Biphenols to Nanographenes. *Angew. Chem., Int. Ed.* **2020**, *59*, 2998. (b) Grzybowski, M.; Skonieczny, K.; Butenschon, H.; Gryko, D. T. Comparison of Oxidative Aromatic Coupling and the Scholl Reaction. *Angew. Chem., Int. Ed.* **2013**, *52*, 9900. (c) Jolly, A.; Miao, D.; Daigle, M.; Morin, J. F. Emerging Bottom-Up Strategies for the Synthesis of Graphene Nanoribbons and Related Structures. *Angew. Chem., Int. Ed.* **2020**, *59*, 4624. (d) Zhu, C.; Wang, D.; Wang, D.; Zhao, Y.; Sun, W. Y.; Shi, Z. Bottom-up Construction of pi-Extended Arenes by a Palladium-Catalyzed Annulative Dimerization of *o*-Iodobiaryl Compounds. *Angew. Chem., Int. Ed.* **2018**, *57*, 8848. (e) Lu, D.; Zhuang, G.; Wu, H.; Wang, S.; Yang, S.; Du, P. A Large pi-Extended Carbon Nanoring Based on Nanographene Units: Bottom-Up Synthesis, Photophysical Properties, and Selective Complexation with Fullerene C(70). *Angew. Chem., Int. Ed.* **2017**, *56*, 158.

(4) (a) Liu, Z.; Fu, S.; Liu, X.; Narita, A.; Samori, P.; Bonn, M.; Wang, H. I. Small Size, Big Impact: Recent Progress in Bottom-Up Synthesized Nanographenes for Optoelectronic and Energy Applications. *Adv. Sci.* **2022**, *9*, No. e2106055. (b) Baier, D. M.; Gratz, S.; Jahromi, B. F.; Hellmann, S.; Bergheim, K.; Pickhardt, W.; Schmid, R.; Borchardt, L. Beyond the Scholl Reaction - One-step Planarization and Edge Chlorination of Nanographenes by Mechanochemistry. *RSC Adv.* **2021**, *11*, 38026. (c) Lungerich, D.; Papaianina, O.; Feofanov, M.; Liu, J.; Devarajulu, M.; Troyanov, S. I.; Maier, S.; Amsharov, K. Dehydrative pi-Extension to Nanographenes with Zig-zag Edges. *Nat. Commun.* **2018**, *9*, 4756. (d) Oró, A.; Romeo-Gella, F.; Perles, J.; Fernández-García, J. M.; Corral, I.; Martín, N. Tetrahedraphene: A Csp(3)-Centered 3D Molecular Nanographene Showing Aggregation-Induced Emission. *Angew. Chem., Int. Ed.* **2023**, *62*, No. e202312314.

(5) (a) Lombardi, F.; Lodi, A.; Ma, J.; Liu, J.; Slota, M.; Narita, A.; Myers, W. K.; Müllen, K.; Feng, X.; Bogani, L. Quantum Units from the Topological Engineering of Molecular Graphenoids. *Science* **2019**, *366*, 1107. (b) Majewski, M. A.; Stępień, M. Bowls, Hoops Saddles: Synthetic Approaches to Curved Aromatic Molecules. *Angew. Chem., Int. Ed.* **2019**, *58*, 86. (c) Rickhaus, M.; Mayor, M.; Juríček, M. Chirality in Curved Polyaromatic Systems. *Chem. Soc. Rev.* **2017**, *46*, 1643. (d) Zhang, Y.; Pun, S. H.; Miao, Q. The Scholl Reaction as a Powerful Tool for Synthesis of Curved Polycyclic Aromatics. *Chem. Rev.* **2022**, *122*, 14554. (e) Fernández-García, J. M.; Evans, P. J.; Medina Rivero, S.; Fernández, I.; García-Fresnadillo, D.; Perles, J.; Casado, J.; Martín, N. pi-Extended Corannulene-Based Nanographenes: Selective Formation of Negative Curvature. *J. Am. Chem. Soc.* **2018**, *140*, 17188.

(6) (a) Fernández-García, J. M.; Izquierdo-García, P.; Buendía, M.; Filippone, S.; Martín, N. Synthetic Chiral Molecular Nanographenes: The Key Figure of the Racemization Barrier. *Chem. Commun.* **2022**, *58*, 2634. (b) Fernández-García, J. M.; Evans, P. J.; Filippone, S.; Herranz, M. A.; Martín, N. Chiral Molecular Carbon Nanostructures. *Acc. Chem. Res.* **2019**, *52*, 1565. (c) Anderson, H. V.; Gois, N. D.; Chalifoux, W. A. New Advances in Chiral Nanographene Chemistry. *Org. Chem. Front.* **2023**, *10*, 4167.

(7) (a) Schnitzlein, M.; Shoyama, K.; Würthner, F. A Highly Fluorescent Bora[6]helicene Exhibiting Circularly Polarized Light Emission. *Chem. Sci.* **2024**, *15*, 2984−2989. (b) Niu, W.; Fu, Y.; Deng, Q.; Qiu, Z. L.; Liu, F.; Popov, A. A.; Komber, H.; Ma, J.; Feng, X. Enhancing Chiroptical Responses in Helical Nanographenes via Geometric Engineering of Double [7]Helicenes. *Angew. Chem., Int. Ed.* **2024**, *63*, No. e202319874. (c) Qiu, Z.; Ju, C. W.; Frederic, L.; Hu, Y.; Schollmeyer, D.; Pieters, G.; Müllen, K.; Narita, A. Amplification of Dissymmetry Factors in pi-Extended [7]- and [9]Helicenes. *J. Am. Chem. Soc.* **2021**, *143*, 4661.

(8) (a) Liu, X.; Jin, Z.; Qiu, F.; Guo, Y.; Chen, Y.; Sun, Z.; Zhang, L. Hexabenzoheptacene: A Longitudinally Multihelicene Nanocarbon with Local Aromaticity and Enhanced Stability. *Angew. Chem., Int. Ed.* **2024**, *63*, No. e202407547. (b) Zhu, Y.; Wang, J. Helical Synthetic Nanographenes with Atomic Precision. *Acc. Chem. Res.* **2023**, *56*, 363. (c) Peng, L. J.; Wang, X. Y.; Li, Z. A.; Gong, H. Y. All Carbon Helicenes and π-Extended Helicene Derivatives. *Asian J. Org. Chem.* **2023**, *12*, No. e202300543. (d) Izquierdo-García, P.; Fernández-García, J. M.; Perles, J.; Fernández, I.; Martín, N. Electronic Control of the Scholl Reaction: Selective Synthesis of Spiro vs Helical Nanographenes. *Angew. Chem., Int. Ed.* **2023**, *62*, No. e202215655.

(9) (a) Navakouski, M.; Zhylitskaya, H.; Chmielewski, P. J.; Lis, T.; Cybińska, J.; Stępień, M. Stereocontrolled Synthesis of Chiral Heteroaromatic Propellers with Small Optical Bandgaps. *Angew. Chem., Int. Ed.* **2019**, *58*, 4929. (b) Zhu, Y.; Guo, X.; Li, Y.; Wang, J. Fusing of Seven HBCs toward a Green Nanographene Propeller. *J. Am. Chem. Soc.* **2019**, *141*, 5511. (c) Izquierdo-García, P.; Fernández-García, J. M.; Fernández, I.; Perles, J.; Martín, N. Helically Arranged Chiral Molecular Nanographenes. *J. Am. Chem. Soc.* **2021**, *143*, 11864.

(10) (a) Yang, L.; Ju, Y. Y.; Medel, M. A.; Fu, Y.; Komber, H.; Dmitrieva, E.; Zhang, J. J.; Obermann, S.; Campaña, A. G.; Ma, J.; Feng, X. Helical Bilayer Nonbenzenoid Nanographene Bearing a [10]Helicene with Two Embedded Heptagons. *Angew. Chem., Int. Ed.* **2023**, *62*, No. e202216193. (b) Niu, W.; Fu, Y.; Qiu, Z. L.; Schurmann, C. J.; Obermann, S.; Liu, F.; Popov, A. A.; Komber, H.; Ma, J.; Feng, X. pi-Extended Helical Multilayer Nanographenes with Layer-Dependent Chiroptical Properties. *J. Am. Chem. Soc.* **2023**, *145*, 26824. (c) Ju, Y. Y.; Chai, L.; Li, K.; Xing, J. F.; Ma, X. H.; Qiu, Z. L.; Zhao, X. J.; Zhu, J.; Tan, Y. Z. Helical Trilayer Nanographenes with Tunable Interlayer Overlaps. *J. Am. Chem. Soc.* **2023**, *145*, 2815. (d) Evans, P. J.; Ouyang, J.; Favereau, L.; Crassous, J.; Fernández, I.; Perles, J.; Martín, N. Synthesis of a Helical Bilayer Nanographene. *Angew. Chem., Int. Ed.* **2018**, *57*, 6774.

(11) Li, G.; Luican, A.; Lopes dos Santos, J. M. B.; Castro Neto, A. H.; Reina, A.; Kong, J.; Andrei, E. Y. Observation of Van Hove Singularities in Twisted Graphene Layers. *Nat. Phys.* **2010**, *6*, 109.

(12) Cao, Y.; Fatemi, V.; Fang, S.; Watanabe, K.; Taniguchi, T.; Kaxiras, E.; Jarillo-Herrero, P. Unconventional Superconductivity in Magic-angle Graphene Superlattices. *Nature* **2018**, *556*, 43.

(13) Izquierdo-García, P.; Fernández-García, J. M.; Medina Rivero, S.; Sámal, M.; Rybáček, J.; Bednárová, L.; Ramírez-Barroso, S.; Ramírez, F. J.; Rodríguez, R.; Perles, J.; García-Fresnadillo, D.; Crassous, J.; Casado, J.; Stará, I. G.; Martín, N. Helical Bilayer Nanographenes: Impact of the Helicene Length on the Structural, Electrochemical, Photophysical, and Chiroptical Properties. *J. Am. Chem. Soc.* **2023**, *145*, 11599.

(14) (a) Chiesa, A.; Privitera, A.; Macaluso, E.; Mannini, M.; Bittl, R.; Naaman, R.; Wasielewski, M. R.; Sessoli, R.; Carretta, S. Chirality-Induced Spin Selectivity: An Enabling Technology for Quantum Applications. *Adv. Mater.* **2023**, *35*, No. e2300472. (b) Bloom, B. P.; Paltiel, Y.; Naaman, R.; Waldeck, D. H. Chiral Induced Spin Selectivity. *Chem. Rev.* **2024**, *124*, 1950.

(15) Buendía, M.; Fernández-García, J. M.; Perles, J.; Filippone, S.; Martín, N. Enantioselective Synthesis of a Two-fold Inherently Chiral Molecular Nanographene. *Nat. Synth.* **2024**, *3*, 545.

(16) Morita, F.; Kishida, Y.; Sato, Y.; Sugiyama, H.; Abekura, M.; Nogami, J.; Toriumi, N.; Nagashima, Y.; Kinoshita, T.; Fukuhara, G.; Uchiyama, M.; Uekusa, H.; Tanaka, K. Design and Enantioselective Synthesis of 3D π-Extended Carbohelicenes for Circularly Polarized Luminescence. *Nat. Synth.* **2024**, *3*, 774.

(17) (a) Tkachenko, N. V.; Scheiner, S. Optical Stability of 1,1′-Binaphthyl Derivatives. *ACS Omega* **2019**, *4*, 6044. (b) Li, S.; Li, R.; Zhang, Y. K.; Wang, S.; Ma, B.; Zhang, B.; An, P. BINOL-like Atropisomeric Chiral Nanographene. *Chem. Sci.* **2023**, *14*, 3286.

(18) Nakanishi, K.; Fukatsu, D.; Takaishi, K.; Tsuji, T.; Uenaka, K.; Kuramochi, K.; Kawabata, T.; Tsubaki, K. Oligonaphthofurans: Fan-Shaped and Three-Dimensional π-Compounds. *J. Am. Chem. Soc.* **2014**, *136*, 7101.

(19) Areephong, J.; Ruangsupapichart, N.; Thongpanchang, T. A Concise Synthesis of Functionalized 7-oxa-[5]Helicenes. *Tetrahedron Lett.* **2004**, *45*, 3067.

(20) (a) Guido, C. A.; Zinna, F.; Pescitelli, G. CPL Calculations of [7]Helicenes with Alleged Exceptional Emission Dissymmetry Values. *J. Mater. Chem. C* **2023**, *11*, 10474. (b) Zhang, L.; Song, I.; Ahn, J.; Han, M.; Linares, M.; Surin, M.; Zhang, H.-J.; Oh, J. H.; Lin, J. π-Extended Perylene Diimide Double-heterohelicenes as Ambipolar Organic Semiconductors for Broadband Circularly Polarized Light Detection. *Nat. Commun.* **2021**, *12*, 142. (c) Cei, M.; Di Bari, L.; Zinna, F. Circularly Polarized Luminescence of Helicenes: A Data-informed Insight. *Chirality* **2023**, *35*, 192.

(21) Reger, D.; Haines, P.; Amsharov, K. Y.; Schmidt, J. A.; Ullrich, T.; Bonisch, S.; Hampel, F.; Gorling, A.; Nelson, J.; Jelfs, K. E.; Guldi, D. M.; Jux, N. A Family of Superhelicenes: Easily Tunable, Chiral Nanographenes by Merging Helicity with Planar pi Systems. *Angew. Chem., Int. Ed.* **2021**, *60*, 18073.

(22) Zhou, Z.; Fernández-García, J. M.; Zhu, Y.; Evans, P. J.; Rodríguez, R.; Crassous, J.; Wei, Z.; Fernández, I.; Petrukhina, M. A.; Martín, N. Site-Specific Reduction-Induced Hydrogenation of a Helical Bilayer Nanographene with K and Rb Metals: Electron Multiaddition and Selective Rb(+) Complexation. *Angew. Chem., Int. Ed.* **2022**, *61*, No. e202115747.

https://doi.org/10.1021/jacs.4c14544
J. Am. Chem. Soc. 2024, 146, 34943−34949